N. Jb. Miner. Abh. Fast Track DOI: 10.1127/0077-7757/2006/0058

Fast Track Article

Coeval late-Variscan emplacement of granitic rocks: an example from the Regensburg Forest, NE Bavaria

Wolfgang Siebel, Horst Peter Hann, Cosmas Kongnyuy Shang (Tübingen), **Johann Rohrmüller** (Marktredwitz), and **Fukun Chen** (Beijing)

With 6 figures and 5 tables

Abstract: Detailed field mapping in the Regensburg Forest, West Bohemian Massif, has enabled us to trace the distribution of a group of minor intrusions (granodiorites, granite porphyry dykes, two-mica granites). In order to unravel their genetic relation and to constrain their age, geochemical and geochronological studies were carried out. $^{207}Pb/^{206}Pb$ evaporation analyses of zircons gave ages of 324 ± 2 Ma for a granodiorite (Stallwang granodiorite), and 323 ± 2 Ma for a granite porphyry dyke. U–Th–Pb dating of monazite from a two-mica granite body gave concordant ages of 323 ± 4 Ma (average $^{207}Pb/^{235}U$-age), 322 ± 5 Ma (average $^{206}Pb/^{238}U$-age) and 323 ± 5 Ma (average $^{208}Pb/^{232}Th$-age). All these ages define the crystallization times and therefore reflect the simultaneous emplacement of the granitoids. The age determination was largely complicated by the predominance of inherited zircon cores. Combining zircon geochronology with geochemical and Sr–Nd data, it becomes evident that the granitoids were derived from Palaeozoic crustal protoliths which, in turn, contain components from Proterozoic (or older) rocks. A source-rock evaluation based on major element oxides allows discriminating between different protoliths. Lithological compositions similar to presently exposed country rock gneisses (mainly greywacke transformed into more or less homogeneous diatexite) are a potential source for the two-mica granites. The geochemistry of the granite porphyry dykes and the granodiorite is consistent with the experimental results of melting mafic pelitic and amphibolitic protoliths, respectively.

Key words: geochemistry, geochronology, granite, petrogenesis, Regensburg Forest, Variscan magmatism, zircon.

1. Introduction and geological problem

The Regensburg Forest (northwest Bavarian Forest) forms part of the Moldanubian basement at the western margin of the Bohemian Massif. It is bounded by the Bavarian Pfahl zone in the NE and by the Danube fault zone in the SW (Fig. 1). As a segment of the Variscan orogenic belt, which resulted from the collision of Laurasia, Gondwana and several microplates (Matte 1986, 2001, Franke et al. 1995, Tait et al. 1997, McKerrow et al. 2000), the Regensburg Forest comprises a supracrustal rock assemblage of the Moldanubian Monotonous Series. Deposition of the sedimentary precursors (greywackes and pelites intercalated with minor quartzitic rocks and calc-silicates) took place between 600 and 490 Ma (Grauert et al. 1974, Gebauer et al. 1989, Teipel et al. 2004). During the late Neoproterozoic and early Ordovician, these sequences were locally intruded by mafic and felsic plutonic rocks (Teipel et al. 2004). Sedimentary and magmatic sequences experienced polyphase metamorphism during the Palaeozoic and were transformed into foliated gneisses, migmatites and more or less homogeneous diatexites (Andritzky 1962, Propach 1977, Propach et al. 2000, Kalt et al. 1999). During the Carboniferous, crustal anatexis culminated and led to the formation of granitic magmas (Finger et al. 1997, Henk et al. 2000). In the Regensburg Forest a well-known product of this melting event is the Kristallgranite I (term coined by Gümbel 1868), a coarse-grained granite with large phenocrysts of K-feldspar (Fischer 1959, Kraus 1962, Köhler & Müller-Sohnius 1986, Propach 1977, 1989). Minor magmatic rocks in the region comprise granodiorites, two-mica granites and granite porphyry dykes. This contribution is an attempt to outline the distribution of these intrusions and to constrain their origin and crystallization time using major

DOI: 10.1127/0077-7757/2006/0058
0077-7757/06/0058 $ 3.50

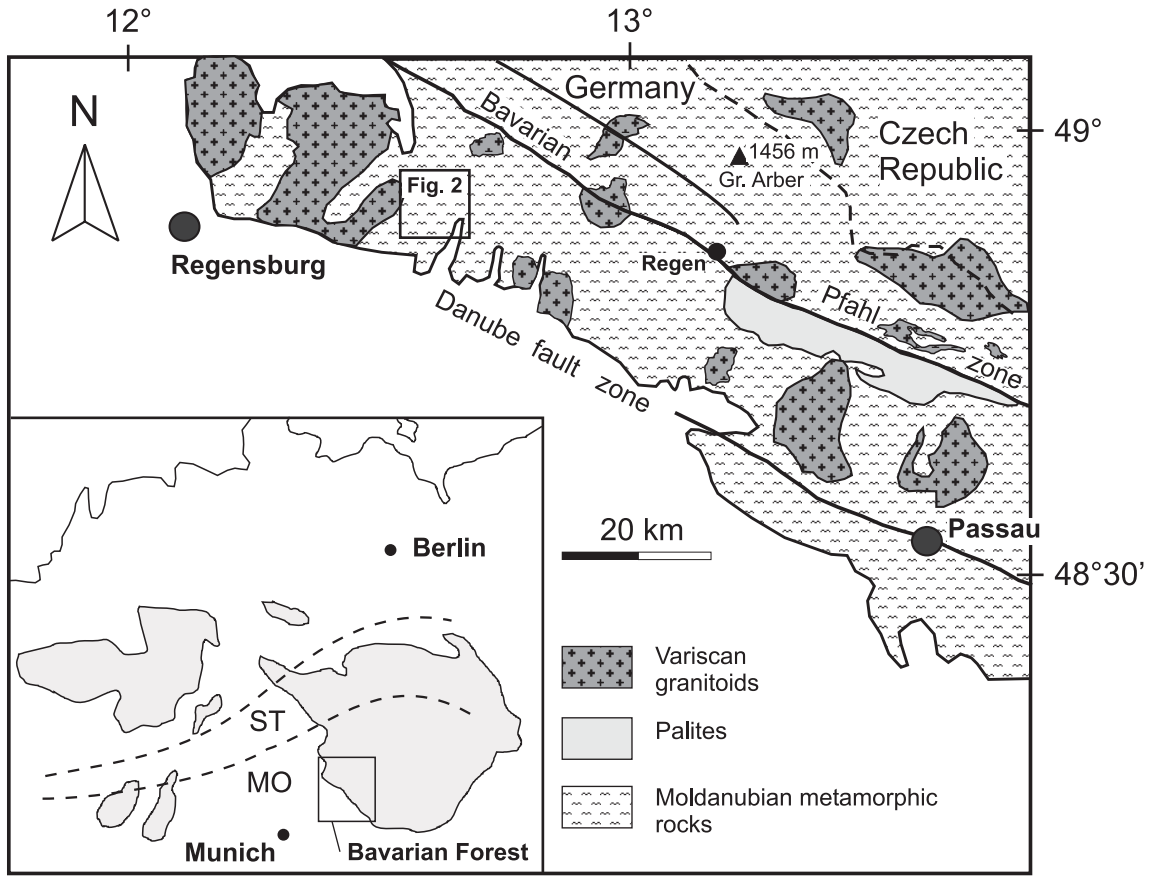

Fig. 1. Simplified geological map of the Bavarian Forest, Western Bohemian Massif, showing the distribution of late-Variscan magmatic rocks. Inset shows the location of the study area (map sheet 6941 Stallwang) within the Regensburg Forest.

and trace element geochemistry, Sr–Nd isotopes, U–(Th)–Pb, and Pb–Pb geochronology.

2. Field description and petrography

All of the investigated granitoids occur within the area of the 1 : 25000 map sheet Stallwang, located approximately 40 km east of the city of Regensburg (Fig. 1). The distribution of these rocks was recently established by Hann (2005) in the framework of a geological mapping project (Fig. 2). A granodiorite, previously known as Stallwang granodiorite, forms several bodies elongated in a NW–SE direction. The largest body has a dimension of 2 km × 350 m. The granodiorite consists of plagioclase (andesine-labradorite), biotite, quartz and K-feldspar with accessory zircon, apatite, titanite and opaque phases (Fig. 3 A). It is host of abundant enclaves of magmatic and sedimentary origin (Griebel 1970). Large K-feldspar crystals with reaction rims and ovoidal to idiomorphic shapes (Fig. 3 B) also occur and have been interpreted as xenoliths derived from a magmatic precursor (Troll 1967, Griebel 1970). The granodiorite has a jointing pattern which made the rocks suitable for quarrying. The sample taken for dating was collected from the abandoned Kirchenberg quarry, 1 km N of Pilgramsberg (for location see Fig. 2). A detailed petrographic examination of the rocks from this locality was carried out by Troll (1967) and Griebel (1970).

The two-mica granite forms several lenses or occurs in a large body of leucocratic granite. The granite was first described by Endlicher (1968) but its exact surface distribution was established during recent field mapping (Hann 2005). The granite crops out mainly NE and SW of the granodiorite (Fig. 2). The largest body is 2 km thick and 3 km long. The two-mica granite is homogeneous, fine- to medium-grained, equigranular and hypidiomorphic and made up of plagioclase, K-feldspar, quartz, biotite, muscovite ± monazite ± zircon ± opaque minerals. Muscovite is a common mineral (Fig. 3 C) and of magmatic origin, providing evidence for a middle to deep crustal emplacement depth of the granite. Where exposed, the granite cuts through the diatexites with sharp contact. Locally, rounded xenoliths of gneiss are

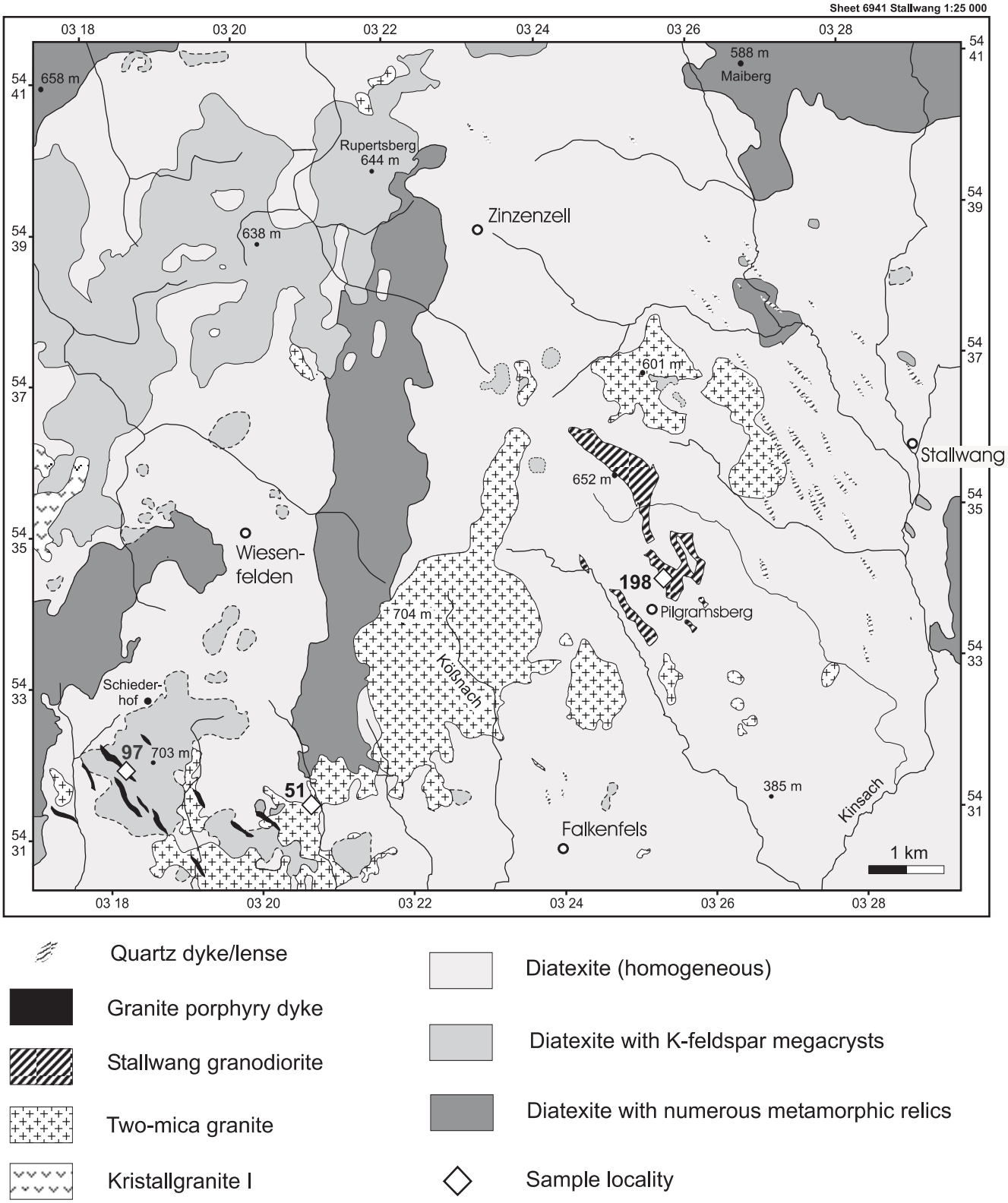

Fig. 2. Geological map sheet 6941 Stallwang, Regensburg Forest (redrawn from HANN 2005). Isotopic analyses were performed on three rock-types (Stallwang granodiorite, two-mica granite, granite porphyry dykes) and the localities from which specimens were dated are indicated.

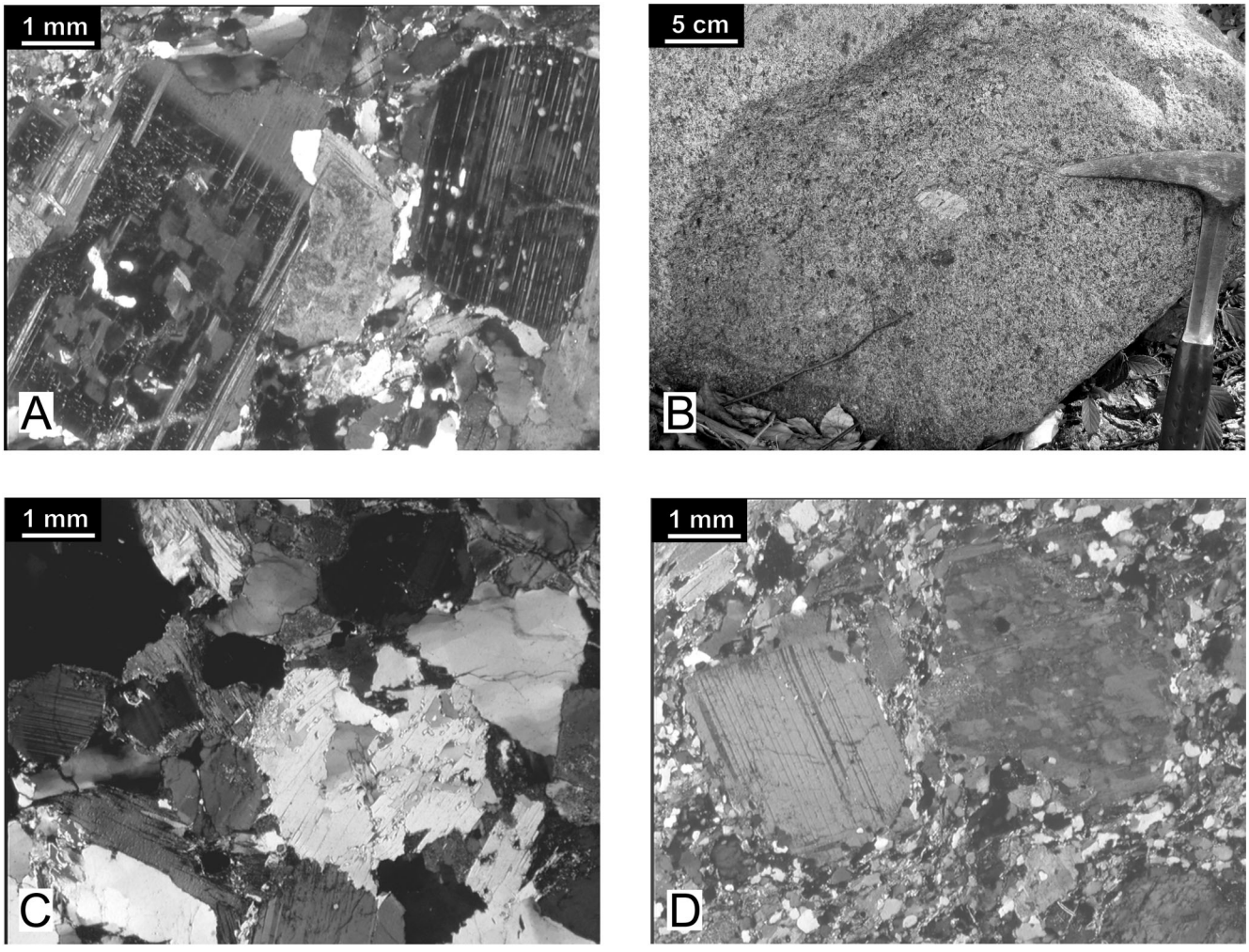

Fig. 3. Rock-types investigated in this study. **A)** Stallwang granodiorite, with twinned plagioclase set in a medium-grained groundmass consisting of feldspar, quartz and biotite; **B)** typical macroscopic appearance of the Stallwang granodiorite; the dark spots are "books" of biotite. A fragment of a single K-feldspar megacryst can be seen in the centre of the photograph; the K-feldspar did not crystallize from the magma, but was incorporated in the melt (see Griebel 1970); **C)** two-mica granite with medium-grained equigranular texture; conspicuous muscovite flake below centre; **D)** granite porphyry dyke with phenocrystic plagioclase (left side) and K-feldspar, (right side). The matrix in between, consisting mostly of quartz, is very fine-grained. All thin section photographs shown in crossed polars.

present in the granite. For isotope analyses, a sample was collected from an outcrop in the southwest part of the main intrusive body, 500 m NE of Auenzell.

In the SW corner of the study area, a number of subvertical granite porphyry dykes occur with a general NW–SE strike. These rocks were first mapped by Endlicher (1968). More detailed mapping and delineation of the boundaries favours the existence of a local dyke swarm consisting of about ten individual dykes (Fig. 2). The dykes have widths of up to 100 m and can be traced along strike for 600 m (Hann 2005). The rocks are more resistent to weathering than the surrounding gneisses and form small linear streaks and ridges. They intersect the diatexites but they also cut the two-mica granites (Fig. 2). Gneissic xenoliths are frequently observed. The dykes are massive, fine-grained rocks composed of feldspar phenocrysts, biotite and quartz macrocrysts, set in a fine-grained groundmass of plagioclase, K-feldspar, quartz, biotite and muscovite (Fig. 3 D) whereby muscovite is inferred as subsolidus alteration product. Accessory minerals include zircon, apatite and opaque minerals. The dykes exhibit a prominent fracture system and they were quarried in the past. The sample taken for dating was collected from an abandoned quarry situated along the western limb of the Kobelberg.

The strike of the granodiorite is NW (160°). The granite porphyry dykes have the same strike direction (Fig. 2). Both intrusions appear to be associated with a crustal

shear zone system referred to as "Stallwanger Furche" (Troll 1967). The magmas intruded from buried fractures oblique to the pronounced NW–SE-trending (120°) Bavarian Pfahl shear zone. Therefore their emplacement age will provide time constraints for the activity of this shear corridor.

3. Analytical procedures

Geochemical and isotopic studies were performed in the laboratories of the Institute of Geosciences, University of Tübingen. Major and trace element concentrations were determined using X-ray fluorescence spectrometry on fused glass beads from whole-rock powders. Measurements were performed on a Bruker AXS S4 Pioneer spectrometer by standard analytical techniques (Potts & Webb 1992). The precision is better than 5 % for major and 10 % for trace elements. Accuracy of individual elemental determinations was tested against international rock standards. For isotope analyses, Rb, Sr, Sm and Nd were isolated by standard ion exchange chromatography (see Chen et al. 2003 for detailed description of procedures). Isotopic measurements of spiked sample loads were made by thermal ionization mass spectrometry (TIMS) on a Finnigan MAT 262 instrument. $^{87}Sr/^{86}Sr$ and $^{143}Nd/^{144}Nd$ ratios were normalised to $^{86}Sr/^{88}Sr = 0.1194$ and to $^{146}Nd/^{144}Nd = 0.7219$, respectively. Total procedural blanks were < 160 pg for Sr and < 80 pg for Nd. Analyses of the La Jolla Nd standard gave a mean value of $^{143}Nd/^{144}Nd = 0.511830 \pm 0.000007$ (n = 8). The NBS 987 Sr standard yielded a $^{87}Sr/^{86}Sr$ ratio of 0.710252 ± 0.000012 (n = 14). Analytical techniques for zircon Pb-evaporation (Kober 1986, 1987) are described in Siebel et al. (2003). The U-Pb zircon analyses were carried out by standard isotope dilution methods as described in Chen and Siebel (2004). U–Pb raw mass-spectrometric

Table 1. Major (in wt.%) and trace element (in ppm) concentrations.

	Granodiorite		Two-mica granite				Granite porphyry dykes		
	ST192	ST198	ST85	ST51	ST278 b	ST278 a	ST98	ST90	ST97
SiO_2	64.90	65.39	71.46	71.65	71.93	73.38	70.05	70.19	70.30
TiO_2	1.21	1.10	0.21	0.40	0.21	0.22	0.60	0.60	0.57
Al_2O_3	15.32	14.99	14.16	14.55	14.34	13.98	14.70	14.58	14.54
Fe_2O_3	5.74	5.41	1.42	2.56	1.53	2.57	3.19	3.37	3.30
MnO	0.083	0.081	0.015	0.033	0.030	0.04	0.043	0.048	0.046
MgO	1.84	1.55	0.37	0.75	0.38	0.37	0.87	0.99	0.90
CaO	2.67	2.59	0.56	0.97	0.57	0.55	1.32	1.10	1.21
Na_2O	3.07	3.30	3.02	3.02	2.96	2.93	3.04	2.99	2.87
K_2O	4.10	4.25	5.36	5.01	6.02	5.98	5.25	5.12	5.27
P_2O_5	0.532	0.52	0.357	0.281	0.30	0.30	0.216	0.21	0.22
LOI	0.68	0.53	0.88	0.55	0.62	0.27	0.71	0.93	0.71
Sum	100.15	99.71	97.81	99.77	98.89	100.59	99.99	100.13	99.94
Ba	1147	1012	241	423	306	303	816	804	770
Rb	156	185	309	288	265	299	250	254	250
Sr	250	226	59	101	56	57	145	145	152
V	75	63	4.2	27	14	12	37	43	38
Y	59	56	9	9	14	16	44	43	43
Zn	81	116	52	97	32	30	52	59	75
Zr	479	427	111	167	117	111	407	359	376
Ce	141	130	30	68	52	41	150	141	148
Eu	1.3	1.2	0.2	0.4	0.3	0.2	0.8	0.8	1.0
La	86	68	29	34	28	14	75	68	60
Nb	38	36	16	18	16	13	29	27	26
Nd	74	72	20	36	26	15	74	59	65
Pb	30	29	25	28	–	–	39	34	38
Sm	11	11	4.8	5.6	6	4.2	9.9	9.6	11
Th	18	14	5.3	21	–	–	37	36	36
Yb	4.9	4.7	0.7	0.7	1.5	1.6	3.5	3.5	3.5
A/CNK	1.07	1.02	1.20	1.20	1.20	1.14	1.12	1.17	1.15

LOI = loss on ignition; A/CNK = mol % $Al_2O_3/(CaO + Na_2O + K_2O)$; – = not measured.

data were processed using the PbDat program (Ludwig 1993).

4. Geochemical composition

Whole-rock geochemical data show a narrow range of composition for each rock-type (Table 1). The most pronounced compositional differences exist between the Stallwang granodiorite and the two types of granites (two-mica granite, granite porphyry dykes). The granodiorite samples are weakly peraluminous, (A/CNK: 1.02 and 1.07), with SiO_2 contents of 64.9 and 65.4 wt.%. The two-mica granites and the granite porphyry dykes are strongly peraluminous, (A/CNK: 1.12–1.20), with SiO_2 contents between 70.0 and 73.4 wt.% (Table 1). The granodiorites have higher TiO_2, Al_2O_3, $Fe_2O_{3\ tot}$, MnO, MgO, CaO, P_2O_5 and lower K_2O concentration compared to the granites. In terms of trace elements the granodiorites have higher Ba, Sr, V, Y, Yb, Zr and lower Rb concentration compared to the granites. Whereas the granodiorites and the granite porphyry dykes have similar concentrations of light rare earth elements, LREE, (La, Ce, Nd, Sm), the two-mica granites are more depleted in LREE.

Geochemical analyses were obtained exclusively from fresh sample material and it seems unlikely that the difference in major and trace element composition between the individual rock-types was caused by alteration processes. More likely, the granites were derived from more differentiated crustal source lithologies compared to the Stallwang granodiorite. Both types of granites have similar geochemical features. However, owing to their higher LREE the granite porphyry dykes cannot represent the final crystallization products of the melt from which the two-mica granite were derived. This is because fractionation of accessory mineral phases normally lowers the LREEs within a granitic melt. As a consequence the granites must have been produced either form different source rocks or by different degrees of partial melting from the same source.

Table 2. U–Pb isotope dilution data for zircons.

Sample/ Fraction	Weight[1] (mg)	$^{206}Pb^{2}/^{204}Pb$	U[1] (ppm)	Pb[1] (ppm)	$^{206}Pb^{*}/^{208}Pb^{*}$	Isotopic ratios[3] $^{206}Pb^{*}/^{238}U$	$^{207}Pb^{*}/^{235}U$	$^{207}Pb^{*}/^{206}Pb^{*}$	Model ages (Ma) $^{206}Pb/^{238}U$	$^{207}Pb/^{235}U$	$^{207}Pb/^{206}Pb$
Granodiorite											
Zr–198–5	0.053	944	5332	294	12.7	0.05294 ±38	0.3878±29	0.05312 ±12	333	333	334
Zr–198–4	0.041	8362	664	43	17.9	0.06755 ±68	0.5180±53	0.05562 ±12	421	424	437
Zr–198–2	0.025	12736	356	27	46.1	0.08250 ±55	0.6579±65	0.05784 ±40	511	513	524
Zr–198–3	0.017	20252	160	63	2.7	0.3003 ±20	6.404 ±44	0.15469 ±17	1693	2033	2398
Two-mica granite											
Zr–51–2	0.478	11280	74	3.4	40.7	0.0495 ±11	0.3614±81	0.05295 ±16	311	313	327
Zr–51–3	0.260	7909	99	5.1	13.7	0.05274 ±41	0.3902±32	0.05366 ±13	331	335	357
Zr–51–9	0.566	11638	111	5.8	11.7	0.05351 ±44	0.3955±33	0.053614±67	336	338	355
Zr–51–1	0.914	17833	148	7.9	14.9	0.055307±31	0.4127±45	0.054120±30	347	351	376
Zr–51–6	0.342	8490	104	5.5	25.5	0.05554 ±51	0.4764±44	0.062215±87	348	396	682
Zr–51–4	0.732	12064	82	5.5	9.4	0.06676 ±70	0.6428±76	0.069824±51	417	504	923
Granite porphyry dyke											
Zr–97–2	0.098	3839	534	27	10.9	0.05144 ±28	0.3762±21	0.053035±61	323	324	330
Zr–97–3	0.060	897	208	12	7.4	0.05150 ±28	0.3794±27	0.05343 ±24	324	327	347
Zr–97–5	0.031	688	333	22	3.6	0.05298 ±30	0.3883±31	0.05315 ±29	333	333	335
Zr–97–8	0.056	1843	543	30	9.9	0.05371 ±39	0.4073±31	0.054995±96	337	347	412
Zr–97–6	0.044	4434	661	39	12.1	0.05891 ±44	0.4319±33	0.053171±93	369	364	336
Zr–97–7	0.025	1619	245	19	7.9	0.07371 ±43	0.5959±50	0.05864 ±34	458	475	554
Zr–97–4	0.044	10408	897	77	12.5	0.08471 ±51	1.001 ±60	0.085706±54	524	704	1332
Zr–97–1	0.091	7974	297	35	11.2	0.11279 ±61	1.886 ±10	0.121311±62	689	1076	1976

* = Radiogenic lead.

[1] Weight and concentration error for individual zircon fraction better than 20%; each fraction originally containing 1–6 grains.

[2] Ratio corrected for mass fractionation and spike contribution.

[3] Ratio corrected for mass fractionation, spike, blank and common Pb (Stacey & Kramers 1975).

All errors given at 2σ.

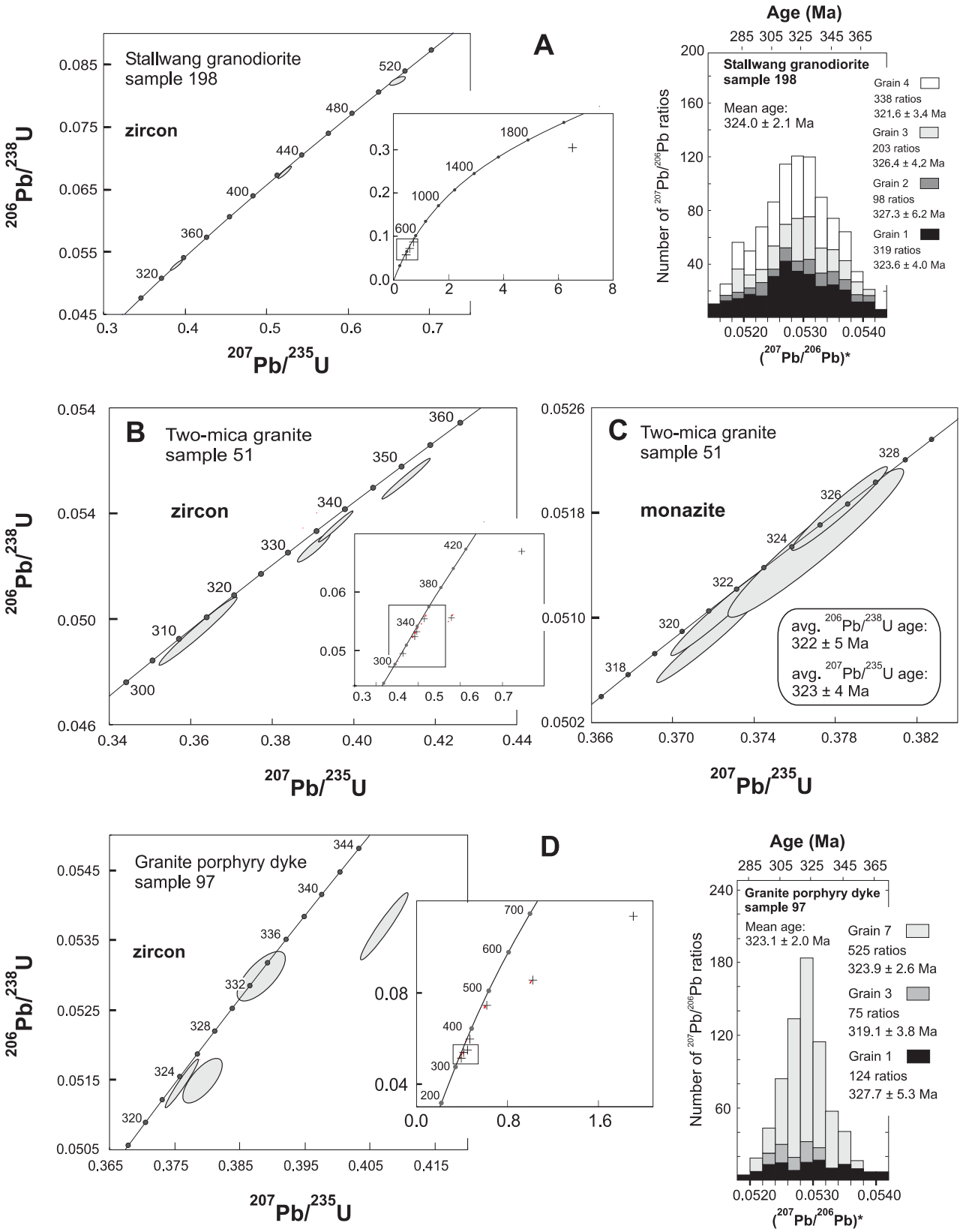

Fig. 4. Plots of U–Pb isotope dilution and Pb–Pb zircon evaporation data. **(A)** Concordia diagram and frequency distribution of $^{207}Pb/^{206}Pb$ ratios derived from zircon evaporation of the Stallwang granodiorite. U–Pb concordia diagram for zircons **(B)** and monazites **(C)** from the two-mica granite. **(D)** U–Pb concordia diagram and frequency distribution of $^{207}Pb/^{206}Pb$ ratios derived from zircon evaporation of a granite porphyry dyke. Drawn error ellipses are 2σ.

5. Geochronology

Granodiorite

Four zircon fractions from the Stallwang granodiorite (sample 198) were analysed by the U–Pb isotope dilution method (Fig. 4 A, Table 2). Only one fraction yields concordant U–Pb ages at 333 Ma. Two fractions are slightly discordant and plot below the concordia curve at ~ 420 Ma and ~ 510 Ma. These fractions probably contain a larger amount of inherited zircon xenocrysts which might reflect an approximate time of early Palaeozoic magmatic activity or they retain a mixture of old lead from several earlier cycle(s) of zircon crystallization. The presence of inherited Proterozoic zircons is suggested by another zircon fraction from the granodiorite which is strongly discordant and gives a $^{207}Pb/^{206}Pb$ age of ~ 2400 Ma. Inherited zircon xenocrysts with U–Pb ages between 2700 and 2000 Ma are known from different regions of the Bavarian Forest (Grauert et al. 1974, Gebauer et al. 1989, Teipel et al. 2004) both from paragneiss and orthogneiss units.

In order to better constrain the intrusion time of the granodiorite, $^{207}Pb/^{206}Pb$ evaporation analyses were performed on 17 individual zircon crystals. Eleven grains turned out to be old giving increasingly older $^{207}Pb/^{206}Pb$ ages for successively higher evaporation temperature steps. The ages of the highest temperature step, which might closely correspond to the age of the core, range from 613 to 421 Ma. In all these grains even the lowest temperature evaporation step was characterised by contribution of old ($^{207}Pb/^{206}Pb$ ages > 340 Ma) lead. Two other zircons gave $^{207}Pb/^{206}Pb$ ages around ~ 335 Ma. Four grains yield very consistent $^{207}Pb/^{206}Pb$ ratios from successively higher evaporation temperature steps indicating that these crystals contained a single lead phase. This consistency strongly supports the view that the grains were free of inherited older lead components. Their mean $^{207}Pb/^{206}Pb$ evaporation age is 324 ± 2 Ma (Fig. 4 A, Table 3) and this age is interpreted as the crystallization age of the granodiorite. A Rb–Sr age on a biotite whole-rock pair indicates cooling through 300–350° at 316.2 ± 3.1 Ma (Table 5).

Two-mica granite

Six analysed zircon fractions from the two-mica granite yielded discordant U–Pb data (Fig. 4 B). Four fractions are only slightly discordant and lie below the concordia curve between 350–310 Ma. The remaining two zircon fractions are more discordant with $^{207}Pb/^{206}Pb$ ages of 923 and 682 Ma. Whereas the older ages are interpreted to be due to analysing composite grains of magmatic and xenocrystic zircons, the young age of one fraction could result from post-crystallization processes, i. e., later lead loss. The uranium (and lead) concentrations of the zircon fractions are lower compared to that of the zircons in the other granitoids (Table 2). This might reflect lower uranium concentration of the two-mica granite melt or sup-

Table 3. $^{207}Pb/^{206}Pb$ evaporation data for single zircons from Stallwang granodiorite and a porphyritic dyke sample.

Sample	no.[1]	$\frac{^{204}Pb}{^{206}Pb}$	$\frac{^{206}Pb^*}{^{208}Pb^*}$	$\frac{Th^2}{U}$	$\frac{^{207}Pb^{*\,3}}{^{206}Pb^*}$	Age (Ma)	error[4] (Ma)
Granodiorite							
Zr–198–1	319	0.000071	7.8	0.40	0.052877 ± 0.000076	323.6	4.0
Zr–198–2	98	0.000054	7.8	0.40	0.052964 ± 0.000035	327.3	6.2
Zr–198–3	203	0.000011	49	0.06	0.052944 ± 0.000081	326.4	4.2
Zr–198–3	338	0.000090	6.8	0.47	0.052832 ± 0.000058	321.6	3.4
Weighted average						**324.0**	**2.1**
Granite porphyry dyke							
Zr–97–1	124	0.000059	20	0.16	0.052973 ± 0.000110	327.7	5.3
Zr–97–2	75	0.000021	23	0.13	0.052772 ± 0.000070	319.1	3.8
Zr–97–3	525	0.000019	55	0.06	0.052884 ± 0.000028	323.9	2.6
Weighted average						**323.1**	**2.0**

[1] Number of measured $^{207}Pb/^{206}Pb$ isotope ratios per grain.

[2] Model ratio calculated from $^{208}Pb/^{206}Pb$ ratio and age of the sample; * = radiogenic lead.

[3] Errors are 2σ standard errors.

[4] Error calculated using following formula: $\sqrt{(2\sigma/\sqrt{n})^2 + \Delta f^2}$ where n is the number of measured $^{207}Pb/^{206}Pb$ isotope ratios. 2σ is the 2-sigma standard error of the Gaussian frequency distribution function and Δf is an assumed uncertainty of the measured $^{207}Pb/^{206}Pb$ ratio of 0.1 %.

Table 4. U–Pb isotope dilution data for monazite.

Sample/ Fraction	Weight[1] (mg)	$^{206}Pb/^{204}Pb$[2]	U[1] (ppm)	Th[1] (ppm)	Pb[1] (ppm)	$^{206}Pb/^{238}U$	Isotopic ratios[3] $^{207}Pb/^{235}U$	$^{208}Pb/^{232}Th$	$^{207}Pb/^{206}Pb$	Model ages (Ma) $^{206}Pb/^{238}U$	$^{207}Pb/^{235}U$	$^{208}Pb/^{232}Th$	$^{207}Pb/^{206}Pb$
Two-mica granite													
Mz–51/1	0.014	1501	5391	46000	933	0.05184±27	0.3782±20	0.016205±86	0.052910±50	326	326	325	325
Mz–51–2	0.064	649	13410	65600	1623	0.05106±28	0.3725±21	0.01590 ±11	0.052906±67	321	321	319	325
Mz–51–4	0.010	811	6735	36070	858	0.05082±26	0.3716±20	0.016133±83	0.053032±63	320	321	323	330
Mz–51–5	0.022	467	2705	17420	402	0.05158±49	0.3771±37	0.01641 ±30	0.05302 ±13	324	325	329	330

[1] Weight and concentration error better than 20 %.
[2] Ratio corrected for mass fractionation and spike contribution.
[3] Ratio corrected for mass fractionation, spike, blank and common Pb (Stacey & Kramers 1975).
All errors given at 2σ.

pression of uranium uptake in zircons by a competing uranium-bearing accessory phase, like monazite, a mineral which is present in the two-mica granite. In order to obtain better time constraints for the two-mica granite we also performed U–Th–Pb analyses on monazite crystals (Fig. 4 C, Table 4). Four fractions gave concordant ages of 323 ± 4 Ma (average $^{207}Pb/^{235}U$ age), 322 ± 5 Ma (average $^{206}Pb/^{238}U$ age) and 323 ± 5 Ma (average $^{208}Pb/^{232}Th$ age) which we interpret to represent the crystallization age of the two-mica granite body. A whole-rock muscovite Rb–Sr analysis gave an age of 328.8 ± 3.4 Ma consistent with the U–Pb-monazite ages within error indicating rapid cooling. A biotite from the same sample gives a Rb–Sr age of 285.6 ± 2.9 Ma. This young date is likely a result of retrograde disturbance of the Rb–Sr biotite system.

Granite porphyry dyke

The eight zircon fractions from this rock-type yielded discordant U–Pb data with $^{207}Pb/^{206}Pb$ ages ranging from 1976 to 330 Ma (Fig. 4 D, Table 2). Due to complexities associated with mixing of inherited and newly grown zircon components as well as possible lead loss, no discordia line can be drawn through the data points. However, two fractions yield nearly concordant U–Pb ages around 324 Ma but without further constraints it is unclear whether this represents the crystallization age of the dykes. Additional age data were obtained by the single zircon Pb-evaporation technique. The $^{207}Pb/^{206}Pb$ ages from three crystals increase with increasing evaporation temperatures. For the highest temperature steps ages of 419 Ma, 632 Ma, and a particular old age of 2327 Ma were obtained. The $^{207}Pb/^{206}Pb$ ratios of three other crystals show no variation with increasing evaporation temperature. Their $^{207}Pb/^{206}Pb$ ages vary between 328 and 319 Ma with a weighted mean age of 323 ± 2 Ma (Fig. 4 D, Table 3). This age which corresponds with two ages from isotope dilution analysis is interpreted as the crystallization age of the granite porphyry dykes.

6. Sr–Nd isotope ratios

Sr and Nd isotope analyses of whole-rock samples and Sr isotope analyses of minerals are given in Table 5. Data for country rock diatexites sampled in the neighbourhood of the granitoids are reported for comparison. The granitoids have initial $^{87}Sr/^{86}Sr$ ratios (calculated for an age of 325 Ma) of 0.7097 (Stallwang granodiorite), 0.7091 (two-mica granite) and 0.7081 (granite porphyry dyke). The $\varepsilon Nd_{323\ Ma}$ values vary in a narrow range between –5.1 and –6.8. The diatexites have Sr and Nd isotope compositions in the same range as the granitoids but they show a larger variation and their isotopic ratios can reach more pronounced crustal values ($^{87}Sr/^{86}Sr_{323\ Ma}$ ratios between 0.707 and 0.716, and $\varepsilon Nd_{323\ Ma}$ between –5.2 to –10.3).

7. Discussion

7.1. Implications from geochronological data for the emplacement age of the granitoids

The observation that U–Pb dilution data from all our investigated granitoid samples are discordant precludes a unique age interpretation from these data alone. The $^{207}Pb/^{206}Pb$ zircon evaporation ages as well as the U–Th–Pb monazite ages have largely constrained the crystallization ages of these rocks. These ages demonstrate that the three different rock-types formed more or less contemporaneously at ~323 Ma. Cross-cutting field rela-

Table 5. Rb–Sr and Sm–Nd isotopic data for granitoids and diatexites.

Sample	$^{87}Rb/^{86}Sr$	$^{87}Sr/^{86}Sr$[1]	$(^{87}Sr/^{86}Sr)_i$[2]	$^{147}Sm/^{144}Nd$	$^{143}Nd/^{144}Nd$[1]	$(^{143}Nd/^{144}Nd)_i$[2]	$\varepsilon Nd_{(t)}$[3]	$T_{DM}(Ga)$[4]
Whole-rock data								
Granitoids (198 = granodiorite, 51 = two-mica granite, 97 = granite porphyry dyke)								
St–198	2.55	0.720298±10	0.70974	0.1087	0.512205±09	0.511961	−5.1	1.5
St–51	8.93	0.750198±08	0.70914	0.1275	0.512147±10	0.511934	−6.8	1.6
St–97	4.92	0.732361±08	0.70807	0.1148	0.512165±10	0.511876	−5.6	1.5
Diatexites								
St–155	10.05	0.753555±10	0.70705	0.1396	0.512169±07	0.511872	−6.8	1.6
St–130	6.10	0.738721±11	0.71048	0.1327	0.512174±05	0.511892	−6.4	1.6
St–291	2.73	0.728996±08	0.71634	0.1228	0.511954±06	0.511693	−10.3	1.9
St–288	1.74	0.716343±09	0.70831	0.1146	0.512199±07	0.511955	−5.2	1.5

Mineral data	$^{87}Rb/^{86}Sr$	$^{87}Sr/^{86}Sr$[1]	whole-rock – mineral age (±2σ error)
St–97 biotite	1370	6.875520±67	316.1±3.2 Ma
St–51 biotite	4568	19.2733 ±19	285.5±2.9 Ma
St–51 musc.	235.2	1.809244±18	328.8±3.4 Ma

[1] Errors are within run errors ($2\sigma_{measured}$).
[2] Initial ratios calculated using the age 325 Ma.
[3] Typical uncertainty in εNd(t) (t = 325 Ma) is ±0.4.
[4] Nd depleted mantle model age (two-stage) with parameters given in Liew & Hofmann (1988).

tionship shows that the granite porphyry dykes intrude the two-mica granite. However, the time interval between these intrusions was probably too short to be resolved with the precision of ages obtained in this study.

Our preferred crystallization age for the minor intrusions from the Regensburg Forest is close to the inferred crystallization age of the Kristallgranite I, (West of Stallwang) and also coincides with the U–Pb age of the Ödwies granodiorite (East of Stallwang, Propach et al. 2000). The intrusions of the granodiorite and the granite porphyry dykes show a prominent NW strike direction (Fig. 2). These structures are related to coeval activity of sinistral shear deformation between the Pfahl zone and the Danube fault zone ("Stallwanger Furche", Troll 1967). The crystallization age of the granitoids can thus be linked to the activity of this shear zone. In the light of recent data, it appears that pluton emplacement in the Moldanubian zone of Bavaria was rather restricted in time and culminated between 325 and 320 Ma (Propach et al. 2000, Chen et al. 2003, Chen & Siebel 2004, Siebel et al. 2005 a, b, Siebel et al. 2006). The magmatic processes operated during a period when a thermal peak of regional metamorphism affected the country rocks as indicated by new zircon, monazite and xenotime growth (Gebauer et al. 1989, Kalt et al. 2000, Teipel et al. 2004). The geochronological data support a model of contemporaneous deformation, metamorphism, and granite magma formation within the crust and can be interpreted as the result of deep burial of crustal lithologies followed by decompression during rapid exhumation of the Moldanubian root zone (Schulmann et al. 2005). Given this synchroneity and the voluminous but short flare-up of granitic magmatism, it becomes more and more likely that heat was induced by an external source and it seems reasonable to assume that a sudden heat input from hot underplated material triggered melting (Bergantz 1989, Kalt et al. 2000).

7.2. Inherited zircons and their significance

The Palaeozoic and Precambrian ages found in some of the zircon fractions clearly reflect the existence of inherited zircon cores. Due to the limitations of the U–Pb and Pb–Pb methods in spatial age resolution of a poly-metamorphic zircon grain the protoliths ages of the minor intrusions remain poorly constrained. The zircon $^{207}Pb/^{206}Pb$ isotope dilution ages and the $^{207}Pb/^{206}Pb$ evaporation ages derived from the highest temperature evaporation steps show a significant age component between 700 and >330 Ma (Fig. 5). The data shown in this figure also suggests the presence of Mesoarchean and Proterozoic zircon components. These older ages are supported by Nd model ages (Table 5) which confirm that a certain quantity of material represented by the granitoids was added to the crust already during pre-Phanerozoic times. It must be mentioned that the age distribution shown in Fig. 5 reflects various mixtures of detrital and magmatic zircon components. The presence of ages > 1900 Ma, however, suggests a Palaeoproterozoic (or older) prove-

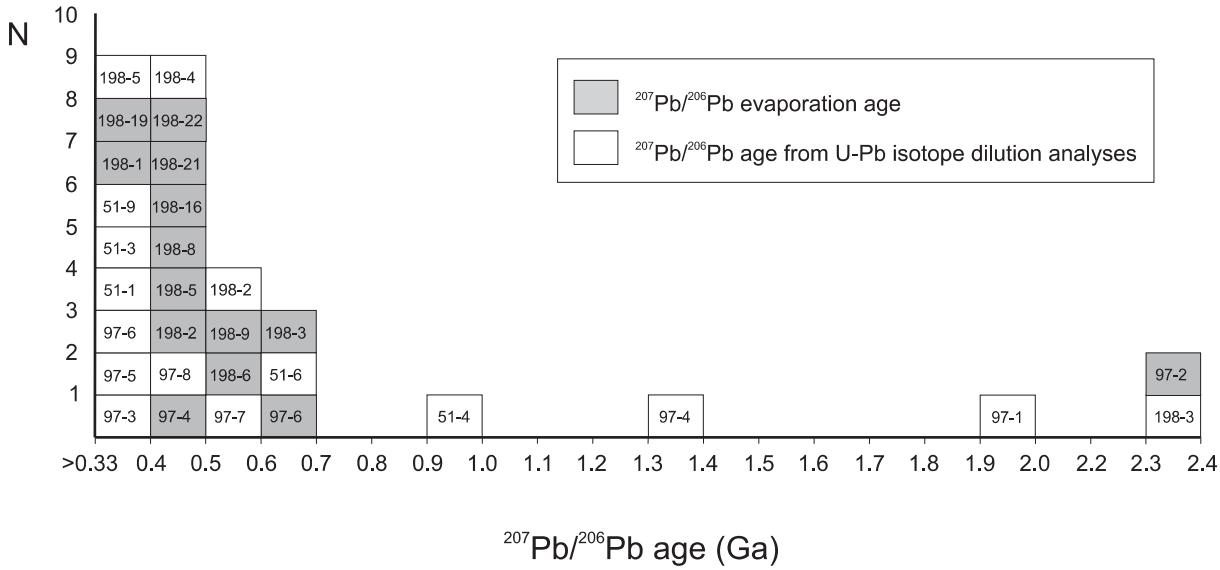

Fig. 5. Histogram displaying the distribution of $^{207}Pb/^{206}Pb$ ages of zircons from the Stallwang granodiorite (sample 198, suffixes denote grain number), two-mica granite (sample 51) and granite porphyry dyke (sample 97). Boxes either represent the $^{207}Pb/^{206}Pb$ age derived from the highest temperature evaporation step of a zircon grain (grey fields) or the $^{206}Pb/^{207}Pb$ isotope dilutions age of a single zircon (white fields). See text for further discussion.

nance for the original sources from which the granites were derived. SHRIMP studies of zircons from paragneisses of the Regensburg Forest and orthogneisses from other parts of the Moldanubian zone of eastern Bavaria yield U–Pb ages mainly in the range between 750–530 Ma (Gebauer et al. 1989) and 550–470 Ma (Teipel et al. 2004) and some grains contain Proterozoic and Archean components. Ages between 750–320 Ma were derived from a paragneiss zircon population in an earlier study (Grauert et al. 1974). The overall detrital zircon age spectrum from exposed metamorphic rocks reported in these studies is similar to the ages presented in Fig. 5. It seems likely, therefore, that the granitoids in the Regensburg Forest were mainly derived from crustal sources with little or no addition of mantle material during their generation.

7.3. Source-rock evaluation

From the limited chemical variation and less evolved composition (i. e. low Rb/Sr ratios) it is evident that the minor intrusions crystallized from less fractionated melts with limited in situ fractional crystallization. Based on their mineralogy, enclave-type, zircon inheritance and Sr–Nd isotope compositions (Table 5) we suggest that the intrusions represent essentially pure crustal melts (see Clemens 2003). Granitoids from adjacent areas (Kristallgranite I, Ödwies granodiorite) were interpreted as products of in situ melting of the adjacent country rock gneisses (Propach 1989, Propach et al. 2000). The following paragraph deals with the geochemical signatures that are to be expected from such source-rock compositions during fluid-absent partial melting process, the most likely process for the generation of S-type magmas (Clemens & Watkins 2001). For the sake of simplicity we do not evaluate magma-mixing models or the addition of juvenile melts from the mantle in this article.

There is a broad overlap in Sr–Nd isotopic composition between the granitoids and their country rock diatexites (Table 5). A partial melting process, however, will normally create Sr–Nd disequilibrium during crustal anatexis (Ayres & Harris 1997, Chavagnac et al. 1999, Tommasini & Davies 1997, Davies & Tommasini 2000, Zeng et al. 2005) and the isotopic composition of the granitoid melt alone cannot simply be used as an isotopic fingerprint of the source. Major oxide and trace element modelling provides an alternative frame to estimate the source-rock characteristics. Constraints on potential source material can be placed by considering experimental melting results (Patiño Douce 1999) from different meta-sedimentary sources that occur in the Regensburg Forest (greywacke, pelite or amphibolite). Melts derived from amphibolites are richer in CaO and have lower total alkalis compared to mica-rich pelitic sources. In contrast, melts derived from muscovite-rich sources are lower in FeO + MgO + TiO_2 compared to those from biotite-rich sources. In Fig. 6 the experimen-

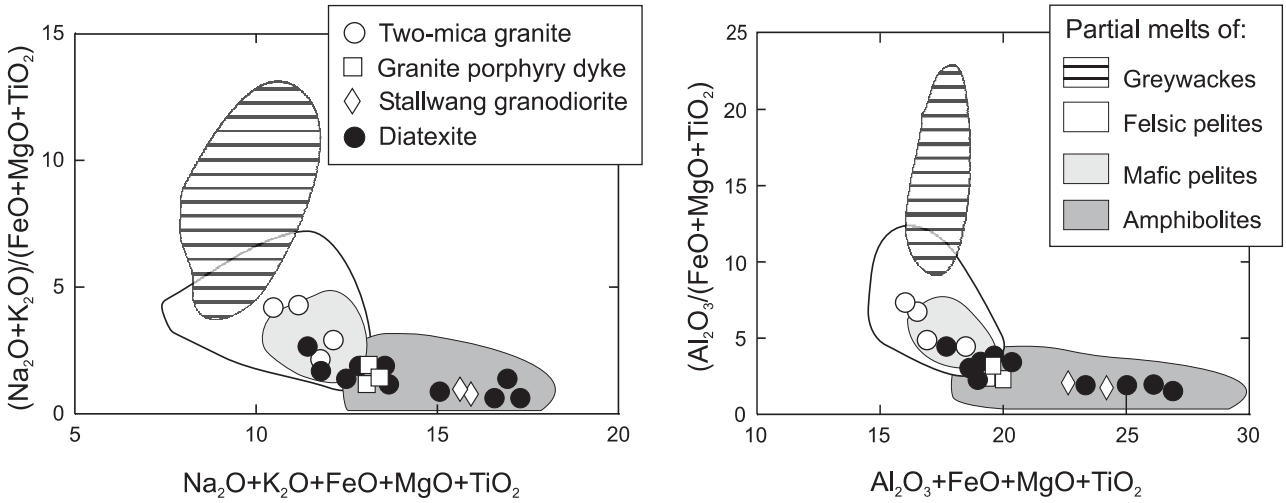

Fig. 6. Chemical composition of minor igneous intrusions from the Regensburg Forest (open symbols) in major oxide diagrams. Samples from diatexite from the same area are shown for comparison (author's unpublished data). Outlined fields denote compositional fields of experimental melts derived from partial melting of felsic pelites, metagreywackes and amphibolites (PATIÑO DOUCE 1999). See text for discussion.

tally derived melt compositions from such rocks are compared with the compositions of the minor intrusions. The latter plot in the compositional field diagnostic for partial melting of amphibolite (Stallwang granodiorite) and mafic pelite (granite porphyry dykes) whereas samples from the two-mica granite extend in the field of felsic pelite. For comparison, geochemical data for diatexites (i. e. characteristic country rocks) are also shown in Fig. 6. These rocks plot along a trajectory similar to that of the minor intrusions. In contrast to granite magma formation, where the partial melt fraction is removed from the crystalline residue, we believe that the diatexite, whose protolith was most likely a greywacke, did not experience significant melt extraction. Partial melting of a diatexite involving melt-residuum separation would, for example, result in more leucocratic melt fraction than represented by the granodiorite and the granite porphyry dykes. We therefore suggest that these intrusions record the melting of other materials than presently exposed diatexites. These intrusions were probably derived from a more mafic protolith. Likely source-rock compositions for these rocks are mafic pelite and/or amphibolites of the Variscan lower crust. The diatexites, however, could represent a more likely progenitor for the two-mica granites.

8. Conclusions

Minor granitic intrusions in the Regensburg Forest yield consistent intrusion ages of ~ 323 Ma, similar to the inferred crystallization age of the nearby Kristallgranite I and Ödwies granite (PROPACH et al. 2000). The narrow range of ages in different rock-types is interpreted as representing an almost synchronous crustal melting event in this region of the Bohemian Massif triggered by an external (mantle lithosphere) heat source. All rocks contain plenty of zircons with older cores resulting in a spectrum of ages that closely resembles zircon systematics in other Moldanubian basement lithologies. The occurrence of a substantial restitic zircon population supports the derivation of the granitoids from crustal precursors. The 700 to > 330 Ma range of $^{207}Pb/^{206}Pb$ apparent ages which are even present within a single sample, results from mixing of different zircon populations (but not necessarily different protoliths) in the magma. Although the granitoids have similar Sr–Nd systematics as the country-rocks, source-rock evaluation shows that only the two-mica granites can be regarded as products of partial melting equivalent to presently exposed diatexites. Sources for the granite porphyry dykes and the Stallwang granite are constrained to be different from exposed diatexites and might comprise mafic pelites and amphibolites of the ancient lower crust.

Acknowledgements

Financial support for this work was provided by the Bayerisches Landesamt für Umwelt, LfU, former BGLA. In this respect, we appreciate Dr. SCHWARZMEIER's effort for granting our petition for geological mapping. G.

Bartholomä, E. Reitter and H. Taubald kindly helped us during the XRF and Sr–Nd isotope analyses. T. Piepenbrink is thanked for sample preparation.

References

Andritzky, G. (1962): Die Anatexis im Regensburger Wald. – N. Jb. Miner. Abh. **99:** 79–112.

Ayres, M. & Harris, N. (1997): REE fractionation and Nd-isotope disequilibrium during crustal anatexis: constraints from Himalayan leucogranites. – Chem. Geol. **139:** 249–269.

Bergantz, G. W. (1989): Underplating and partial melting: Implications for melt generation and extraction. – Science **254:** 1093–1095.

Chavagnac, V., Nägler, T. F. & Kramers, J. D. (1999): Migmatization by metamorphic segregation at subsolidus conditions: Implications for Nd–Pb isotope exchange. – Lithos **46:** 275–298.

Chen, F. & Siebel, W. (2004): Zircon and titanite geochronology of the Fürstenstein granite massif, Bavarian Forest, NW Bohemian Massif: Pulses of late Variscan magmatic activity. – Eur. J. Miner. **16:** 777–788.

Chen, F., Siebel, W. & Satir, M. (2003): Geochemical and isotopic composition and inherited zircon ages as evidence for lower crustal origin of two Variscan S-type granites in the NW Bohemian Massif. – Int. J. Earth Sci. **92:** 173–184.

Clemens, J. D. (2003): S-type granitic magmas – petrogenetic issues, models and evidence. – Earth Sci. Rev. **61:** 1–18.

Clemens, J. D. & Watkins, J. M. (2001): The fluid regime of high-temperature metamorphism during granitoid magma genesis. – Contrib. Mineral. Petrol. **140:** 600–606.

Davies, G. R. & Tommasini, S. (2000): Isotopic disequilibrium during crustal anatexis: implications for petrogenetic studies of magmatic processes. – Chem. Geol. **162:** 169–191.

Endlicher, G. M. (1968): Geologisch-Petrographische Untersuchungen auf dem Südwestviertel des Gradabteilungsblattes Stallwang Nr. 6941. Diploma Thesis, Munich 65 pp.

Finger, F., Roberts, M. P., Haunschmid, B., Schermaier, A. & Steyrer, H. P. (1997): Variscan granitoids of central Europe: their typology, potential sources and tectonothermal relations. – Miner. Petrol. **61:** 67–96.

Fischer, G. (1959): Der Bau des Vorderen Bayerischen Waldes. – Jber. Mitt. Oberrhein. Geol. Ver. NF **41:** 1–22.

Franke, W., Dallmeyer, R. D. & Weber, K. (1995): Geodynamic evolution. – In: Dallmeyer, R. D., Franke, W. & Weber, K. (eds.): Pre-Permian geology of western and central Europe. Springer, Berlin, pp. 579–593.

Gebauer, D., Williams, I. S., Compston, W. & Grünenfelder, M. (1989): The development of the central European continental crust since the Early Archean based on conventional and ion-microprobe dating up to 3.84 b. y. old detrital zircons. – Tectonophysics **157:** 81–96.

Grauert, B., Hänny, R. & Soptrajanova, G. (1974): Age and origin of detrital zircons from the pre-Permian basements of the Bohemian Massif and the Alps. – Contrib. Miner. Petrol. **40:** 105–130.

Griebel, J. (1970): Die Granodiorite von Stallwang und ihre Einschlüsse. – PhD Thesis, Munich, 173 pp.

Gümbel, W. (1868): Geologie von Bayern II: Ostbayerisches Grenzgebirge. Gotha.

Hann, H. P. (2005): Geological map of Bavaria **1:** 25.000 map sheet 6941 Stallwang. LfU, Bavarian national office for environment, Munich.

Henk, A., von Blanckenburg, F., Finger, F., Schaltegger, U. & Zulauf, G. (2000): Syn-convergent high-temperature metamorphism and magmatism in the Variscides: a discussion of potential heat sources. – In: Franke, W., Haak, V., Oncken, O. & Tanner, D. (eds.): Orogenic processes: Quantification and modelling in the Variscan belt. Geol. Soc. London, Spec. Publ. **179:** 387–399.

Kalt, A., Berger, A. & Blümel, P. (1999): Metamorphic evolution of cordierite-bearing migmatites from the Bayerische Wald (Variscan belt, Germany). – J. Petrol. **40:** 601–627.

Kalt, A., Corfu, F., Wijbrans, J. R. (2000): Time calibration of a P-T path from a Variscan high-temperature low-pressure metamorphic complex (Bayerischer Wald, Germany), and the detection of inherited monazite. – Contrib. Miner. Petrol. **138:** 143–163.

Kober, B. (1986): Whole-grain evaporation for $^{207}Pb/^{206}Pb$ age investigations on single zircons using a double-filament thermal ion source. – Contrib. Miner. Petrol. **93:** 481–490.

– (1987): Single-zircon evaporation combined with Pb^{+} emitter-bedding for $^{207}Pb/^{206}Pb$-age investigations using thermal ion mass spectrometry, and implications to zirconology. – Contrib. Miner. Petrol. **96:** 63–71.

Köhler, H. & Müller-Sohnius, D. (1986): Rb-Sr Altersbestimmungen und Sr-Isotopensystematik an Gesteinen des Regensburger Waldes (Moldanubikum NE Bayern) – Teil 2: Intrusivgesteine. – N. Jb. Miner. Abh. **155:** 219–241.

Kraus, G. (1962): Gefüge, Kristallgrößen und Genese des Kristallgranites I im Vorderen Bayerischen Wald. – N. Jb. Miner. Abh. **97:** 357–434.

Liew, T. C. & Hofmann, A. W. (1988): Precambrian crustal components, plutonic associations, plate environment of the Hercynian fold belt of central Europe: indications from a Nd and Sr isotopic study. – Contrib. Miner. Petrol. **98:** 129–138.

Ludwig, K. R. (1993): PBDAT: a computer program for processing Pb–U–Th isotope data, version 1.2, USGS Open-file Report 88–542, 30 pp.

Matte, A. W. (1986): Tectonics and plate tectonics model for the Variscan belt in Europe. – Tectonophysics **126:** 329–374.

– (2001): The Variscan collage and orogeny (480–290 Ma) and the tectonic definition of the Amorican microplate: a review. – Terra Nova **13:** 122–128.

McKerrow, W. S., Mac Niocaill, C., Ahlberg, P. E., Clayton, G., Cleal, C. J., Eagar, R. M. C. (2000): The late Palaeozoic relations between Gondwana and Laurussia. – In: Franke, W., Haak, V., Oncken, O. & Tanner, D. (eds.): Orogenic processes: quantification and modelling in the Variscan belt. – Geol. Soc. London, Spec. Publ. **179:** 9–20.

Patiño Douce, A. E. (1999): What do experiments tell us about the relative contribution of crust and mantle to the origin of granitic magmas? – In: Castro, A., Fernandez, C. & Vigneresse, J. L. (eds.): Understanding granites: Integrating new and classical techniques. Geol. Soc. London, Spec. Publ. **168:** 55–75.

Potts, P. J. & Webb, P. C. (1992): X-ray fluorescence spectrometry. – J. Geochem. Exploration **4:** 251–296.

Propach, G. (1977): Variscan granitization in the Regensburger Wald, West Germany. – N. Jb. Miner. Mh. **1977:** 97–111.

– (1989): The origin of a conformable Variscan granite in Bavaria – Results of geochemical and geochronological investigations. – In: Bonin, B. et al. (eds.): Geochemical and geophysical aspects of the intaractions and evolution of magmas and rocks of the crust. Theophrastus Publications Athens, pp. 193–209.

Propach, G., Baumann, A., Schulz-Schmalschläger, M. & Grauert, B. (2000): Zircon and monazite U–Pb ages of Variscan granitoid rocks and gneisses in the Moldanubian zone of eastern Bavaria, Germany. – N. Jb. Geol. Paläont. Mh. **6:** 345–377.

Schulmann, K., Kröner, A., Hegner, E., Wendt, I., Konopásek, J., Lexa, O. & Stipská, P. (2005): Chronological constraints on the pre-orogenic history, burial and exhumation of deep-seated rocks along the eastern margin of the Variscan orogen, Bohemian Massif, Czech Republic. – Am. J. Sci. **305:** 407–448.

Siebel, W., Blaha, U., Chen, F. & Rohrmüller, J. (2005 a): Geochronology and geochemistry of a dyke-host rock association and implications for the formation of the Bavarian Pfahl shear zone, Bohemian Massif. – Int. J. Earth Sci. **94:** 8–23.

Siebel, W., Chen, F., Satir, M. (2003): Late-Variscan magmatism revisited: New implications from Pb-evaporation zircon ages on the emplacement of redwitzites and granites in NE Bavaria. – Int. J. Earth Sci. **92:** 36–53.

Siebel, W., Reitter, E., Wenzel, T. & Blaha, U. (2005 b): Sr isotope systematics of K-feldspars in plutonic rocks revealed by the Rb/Sr microdrilling technique. – Chem. Geol. **222:** 183–199.

Siebel, W., Thiel, M. & Chen, F. (2006): Zircon geochronology and compositional record of late- to post-kinematic granitoids associated with the Bavarian Pfahl zone (Bavarian Forest). – Miner. Petrol. **86:** 45–62.

Stacey, J. S. & Kramers, J. D. (1975): Approximation of terrestrial lead isotope evolution by a two stage model. – Earth Planet. Sci. Lett. **26:** 207–221.

Tait, J. A., Bachtadse, V., Franke, W. & Soffel, H. C. (1997): Geodynamic evolution of the European Variscan fold belt: palaeomagnetic and geological constraints. – Geol. Rundsch. **86:** 585–598.

Teipel, U., Eichhorn, R., Loth, G., Rohrmüller, J., Höll, R. & Kennedy, A. (2004): U–Pb SHRIMP and Nd isotopic data from the western Bohemian Massif (Bayerischer Wald, Germany): Implications for Upper Vendian and Lower Ordovician magmatism. – Int. J. Earth Sci. **93:** 782–801.

Tommasini, S. & Davies, G. R. (1997): Isotope disequilibrium during anatexis: A case study of contact melting. – Earth Planet. Sci. Lett. **148:** 273–285.

Troll, G. (1967): Die blastokataklastischen Kristallingesteine der Stallwanger Furche, Bayerischer Wald. – Geol. Bavarica **58:** 22–33.

Zeng, L., Asimow, P. D. & Saleeby, J. B. (2005): Coupling of anatectic reactions and dissolution of accessory phases and the Sr and Nd isotope systematics of anatectic melts from a metasedimentary source. – Geochim. Cosmochim. Acta **69:** 3671–3682.

Received: November 26, 2005; accepted: May 8, 2006

Responsible editor: E. Hegner

Author's adress:

W. Siebel, H. P. Hann, C. K. Shang, Institut für Geowissenschaften, Universität Tübingen, Wilhelmstraße 56, 72074 Tübingen, Germany.

J. Rohrmüller, Bayerisches Landesamt für Umwelt, Leopoldstraße 30, 95615 Marktredwitz, Germany.

F. Chen, Laboratory for Radiogenic Isotope Geochemistry, Institute of Geology and Geophysics, Chinese Academy of Sciences, 100029 Beijing, China.